

Sparse Signal Recovery using Log-Sum Regularization and Adaptive Smoothing

Keisuke Morita

Graduate School of Information Sciences,
Tohoku University
Sendai, Japan
mory22k@dc.tohoku.ac.jp

Masayuki Ohzeki

Graduate School of Information Sciences,
Tohoku University
Sendai, Japan
mohzeki@tohoku.ac.jp

Abstract—We study sparse signal recovery from noisy linear observations using nonconvex log-sum regularization. The log-sum penalty reduces the shrinkage bias of ℓ_1 regularization and more closely approximates the ℓ_0 regularization, but its nonconvexity can make reconstruction algorithms unstable. To mitigate this instability, we use an adaptive smoothing strategy that determines the smoothing parameter so that the scalar proximal operator remains continuous. Using this proximal operator, we formulate the approximate message passing (AMP) algorithm and derive the corresponding state evolution (SE) recursion. The fixed point of the SE recursion predicts the final mean squared error (MSE) and, in the noiseless limit, the exact-recovery phase transition. To further investigate finite-dimensional reconstruction behavior, we implement an alternating direction method of multipliers (ADMM) algorithm. In the noiseless setting, we find that the empirical success boundary of ADMM closely agrees with the SE-predicted phase transition. In the noisy setting, we observe that AMP closely follows the SE prediction, whereas ADMM qualitatively reproduces the SE-predicted dependence of the final MSE on the regularization parameter. A comparison with ℓ_1 regularization shows that log-sum regularization is beneficial in low-density or high-measurement-rate regimes, whereas ℓ_1 regularization remains preferable at higher densities and lower measurement rates.

I. INTRODUCTION

Sparse signal recovery aims to reconstruct a high-dimensional signal from incomplete or noisy observations by exploiting the fact that the signal has only a small number of nonzero components in a suitable basis. Compressed sensing is a representative framework for this problem, in which sparse signals are reconstructed from a small number of linear measurements [1], [2]. This formulation arises in applications including astronomy [3], seismic data processing [4], wireless communications [5], and medical image processing [6].

Let $\mathbf{x}^0 \in \mathbb{R}^N$ be the true signal. In a standard noisy linear observation model, we observe

$$\mathbf{y} = \mathbf{A}\mathbf{x}^0 + \mathbf{w}, \quad (1)$$

where $\mathbf{A} \in \mathbb{R}^{M \times N}$ denotes the measurement matrix and $\mathbf{w} \in \mathbb{R}^M$ denotes the noise vector. The goal is to recover \mathbf{x}^0 from

This work has been submitted for consideration to the 2026 International Symposium on Information Theory and Its Applications (ISITA 2026).

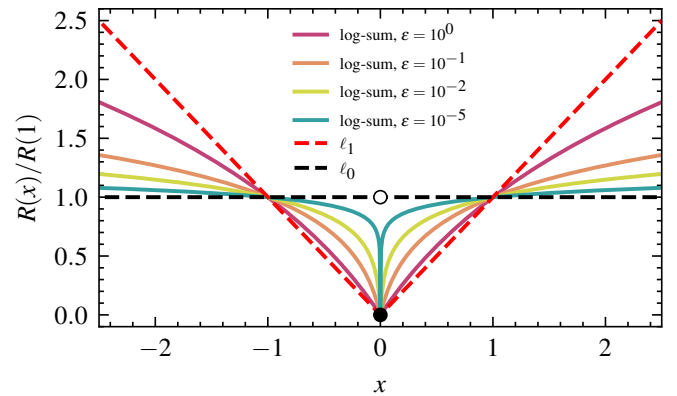


Fig. 1. The normalized log-sum penalty $R(x; \varepsilon)/R(1; \varepsilon)$ as a function of x for various values of ε . The ℓ_1 norm $R(x) = |x|$ and the ℓ_0 pseudo-norm $R(x) = \mathbb{I}_{\{x \neq 0\}}$ are also shown for comparison.

\mathbf{y} and \mathbf{A} . A standard approach is regularized least-squares reconstruction:

$$\min_{\mathbf{x} \in \mathbb{R}^N} \frac{1}{2} \|\mathbf{A}\mathbf{x} - \mathbf{y}\|_2^2 + \lambda_{\text{pen}} \sum_{i=1}^N R_i(x_i), \quad (2)$$

where $\lambda_{\text{pen}} > 0$ is the regularization parameter and $R_i(\cdot)$ is the penalty applied to the i -th component. The ideal sparsity penalty is ℓ_0 regularization, $R_i(x_i) = \mathbb{I}_{\{x_i \neq 0\}}$, which directly penalizes the support size. Since ℓ_0 -regularized reconstruction is computationally difficult, the least absolute shrinkage and selection operator (LASSO), corresponding to ℓ_1 regularization $R_i(x_i) = |x_i|$, is a standard tractable alternative [2], [7]. Its typical performance and phase-transition behavior in compressed sensing have also been studied using statistical-mechanics methods [8]–[11]. Nevertheless, LASSO applies constant shrinkage, which can lead to underestimation of nonzero amplitudes and production of false positives, especially when the number of measurements is limited [12], [13]. This motivates consideration of alternative penalties.

Nonconvex penalties have been studied as alternatives that more closely approximate ℓ_0 regularization while reducing the shrinkage bias of ℓ_1 regularization. Representative examples include ℓ_p ($0 < p < 1$) quasi-norm [14], [15], log-

sum penalty [16]–[18], *smoothly clipped absolute deviation* (SCAD) [12], *minimax concave penalty* (MCP) [19], and *weakly-convex envelope of piecewise penalty* (WEEP) [20]. Previous work has shown that such penalties can reduce bias and enlarge exact-reconstruction regions in compressed sensing [12]–[14], [21], [22]. Because nonconvex penalties make practical optimization sensitive to both the penalty shape and the algorithmic dynamics, several algorithmic strategies based on nonconvexity control and related message-passing methods have been proposed and analyzed [23]–[25].

Among these nonconvex penalties, we focus on log-sum regularization with the penalty function

$$R_i(x_i; \varepsilon) = \log\left(\frac{|x_i|}{\varepsilon} + 1\right), \quad (3)$$

where $\varepsilon > 0$ controls the smoothness of the penalty. As shown in Fig. 1, its normalized form interpolates between ℓ_0 and ℓ_1 : for fixed x_i , $R_i(x_i; \varepsilon)/R_i(1; \varepsilon) \rightarrow \mathbb{I}_{\{x_i \neq 0\}}$ as $\varepsilon \rightarrow 0^+$ and $R_i(x_i; \varepsilon)/R_i(1; \varepsilon) \rightarrow |x_i|$ as $\varepsilon \rightarrow \infty$. The log-sum penalty also has a parameter region where its proximal operator remains continuous, which motivates nonconvexity control that preserves strong sparsity promotion while maintaining algorithmic stability [26].

The main contributions of this work are as follows. First, we formulate an approximate message passing (AMP) algorithm using the scalar proximal operator of the log-sum penalty and derive the state evolution (SE) prediction of its dynamics in the large-system limit. Second, we implement the alternating direction method of multipliers (ADMM) for log-sum regularization and demonstrate that its minimum mean squared error (MSE) and qualitative dependence on λ_{pen} are consistent with the SE prediction. Third, we show that log-sum regularization can outperform ℓ_1 regularization primarily at low signal densities and high measurement rates, while ℓ_1 remains preferable elsewhere.

II. PRELIMINARIES

A. Problem Setting

We consider the following synthetic setting. Each entry of \mathbf{A} is independently generated from a Gaussian distribution with mean 0 and variance $1/N$, and the noise vector \mathbf{w} is generated from a Gaussian distribution with covariance $\sigma^2 \mathbf{I}$. We assume that the true signal \mathbf{x}^0 is sparse and has standard-normal nonzero components:

$$P_{\text{true}}(\mathbf{x}^0) = \prod_{i=1}^N ((1 - \rho)\delta(x_i^0) + \rho\phi(x_i^0)), \quad (4)$$

where $\rho \in [0, 1]$ is the signal density, $\delta(\cdot)$ is the Dirac delta function, and $\phi(\cdot)$ is the density of the standard normal distribution. The expected number of nonzero components is thus $K = \rho N$. Hereafter, we denote $\alpha = M/N$.

B. Adaptive Smoothing of Log-Sum Penalty

Unlike ℓ_1 regularization, log-sum regularization is nonconvex, and algorithmic stability is therefore a practical concern. We use *adaptive smoothing* to address this challenge [26]. To

describe this method, we briefly review the behavior of the proximal operator of the log-sum penalty. For $R_i(x_i; \varepsilon)$, the scalar proximal operator used in AMP and ADMM is

$$\text{prox}_{\lambda_{\text{prox}} R(\cdot)}(h) := \arg \min_{x \in \mathbb{R}} \left\{ \frac{1}{2}(x - h)^2 + \lambda_{\text{prox}} R(x; \varepsilon) \right\}, \quad (5)$$

where $\lambda_{\text{prox}} > 0$ is a positive parameter. The closed-form analysis in [18] has shown that its qualitative behavior is controlled by the relationship between ε and λ_{prox} . If $\varepsilon > \sqrt{\lambda_{\text{prox}}}$, the proximal objective is unimodal and the operator is continuous. In this convex regime, the operator is given by

$$\text{prox}_{\lambda_{\text{prox}} R(\cdot)}(h) = \begin{cases} \text{sign}(h)r_+(|h|) & \text{if } |h| > \lambda_{\text{prox}}/\varepsilon, \\ 0 & \text{otherwise,} \end{cases} \quad (6)$$

where $r_+(|h|) = (|h| - \varepsilon + \sqrt{(|h| + \varepsilon)^2 - 4\lambda_{\text{prox}}})/2$. If $\varepsilon \leq \sqrt{\lambda_{\text{prox}}}$, the objective can have two local minima and the proximal operator becomes discontinuous at the switching threshold $|h| = h_{\text{th}} \in [2\sqrt{\lambda_{\text{prox}}} - \varepsilon, \lambda_{\text{prox}}/\varepsilon]$.

Adaptive smoothing chooses the smoothing parameter ε according to the proximal parameter λ_{prox} by

$$\varepsilon = \sqrt{\lambda_{\text{prox}}} + \Delta_\varepsilon, \quad (7)$$

where $\Delta_\varepsilon > 0$ is a small positive constant. For all numerical experiments in our study, we set $\Delta_\varepsilon = 10^{-10}$ consistently. This rule keeps the proximal operator continuous while retaining strong sparsity-promoting behavior. Because ε changes with λ_{prox} during the algorithm, (2) is not solved with a single fixed ε . As a result, analytical techniques such as the replica method [8], [9], [27] are not directly applicable in this setting.

C. Approximate Message Passing and State Evolution

AMP is an iterative algorithm that computes the expectation of the marginal posterior distribution under the formulation of compressed sensing as a Bayesian estimation problem [28]. AMP iterates as follows:

$$\mathbf{h}^{[t]} = \widehat{\mathbf{x}}^{[t]} + \frac{N}{M} \mathbf{A}^\top \mathbf{z}^{[t]}, \quad (8)$$

$$k^{[t]} = \frac{1}{\alpha} \nabla S\left(\mathbf{h}^{[t]}; \frac{\chi^{[t]} + \lambda_{\text{pen}}}{\alpha} R(\cdot)\right), \quad (9)$$

$$\widehat{\mathbf{x}}^{[t+1]} = S\left(\mathbf{h}^{[t]}; \frac{\chi^{[t]} + \lambda_{\text{pen}}}{\alpha} R(\cdot)\right), \quad (10)$$

$$\mathbf{z}^{[t+1]} = \mathbf{y} - \mathbf{A} \widehat{\mathbf{x}}^{[t+1]} + \mathbf{z}^{[t]} k^{[t]}, \quad (11)$$

$$\chi^{[t+1]} = (\chi^{[t]} + \lambda_{\text{pen}}) k^{[t]}. \quad (12)$$

Here, $\widehat{\mathbf{x}}^{[t]}$ is the estimator, $\mathbf{z}^{[t]}$ is the corrected residual, and $\chi^{[t]}$ represents the effective-noise variance at iteration t . S is the componentwise proximal operator:

$$S(h_i; \lambda R(\cdot)) = \text{prox}_{\lambda R(\cdot)}(h_i). \quad (13)$$

The overline denotes the arithmetic mean over components: $\overline{\nabla S(\mathbf{h}; \cdot)} := \sum_i S'(h_i; \cdot)/N$.

The Onsager correction, the last term in (11), cancels the leading self-interaction term. This cancellation allows

the asymptotic dynamics of AMP with an i.i.d. Gaussian measurement matrix to be characterized by SE [29]. Let the empirical mean squared error (MSE) of AMP at iteration t be

$$E^{[t]} = \frac{1}{N} \left\| \mathbf{x}^{[t]} - \mathbf{x}^0 \right\|_2^2. \quad (14)$$

In the $N, M, K \rightarrow \infty$ limit with $\alpha \rightarrow M/N = O(1)$ and $\rho \rightarrow K/N = O(1)$, the corresponding large-system dynamics are characterized by the following SE recursions:

$$h_*^{[t]} = x^0 + \sqrt{\sigma^2 + \frac{E^{[t]}}{\alpha}} z, \quad (15)$$

$$k_*^{[t]} = \frac{1}{\alpha} \mathbb{E}_{x^0, z} \left[S' \left(h_*^{[t]}; \frac{\chi^{[t]} + \lambda_{\text{pen}}}{\alpha} R(\cdot) \right) \right], \quad (16)$$

$$E^{[t+1]} = \mathbb{E}_{x^0, z} \left[\left(S \left(h_*^{[t]}; \frac{\chi^{[t]} + \lambda_{\text{pen}}}{\alpha} R(\cdot) \right) - x^0 \right)^2 \right], \quad (17)$$

$$\chi^{[t+1]} = (\chi^{[t]} + \lambda_{\text{pen}}) k_*^{[t]}. \quad (18)$$

Here, the expectation is over the true-signal distribution of x^0 and an independent standard Gaussian variable z .

A fixed point of (15)–(18) predicts the final MSE. Because the log-sum penalty is nonconvex, multiple fixed points may exist in some parameter regimes [26]. The actual algorithm can therefore converge to different fixed points depending on the initialization and iteration history. In the experiments, we used the AMP initialization $\hat{\mathbf{x}}^{[0]} = \mathbf{0}$ and $\chi^{[0]} = 1$, and the corresponding SE initialization $E^{[0]} = \mathbb{E}[(x^0)^2]$ and $\chi^{[0]} = 1$.

The expectations in the SE recursions were numerically evaluated as described below. The integration domain was split at the threshold points of the scalar proximal operator, and the contributions from the $x^0 = 0$ and $x^0 \neq 0$ cases were evaluated separately. For the log-sum penalty, the Gaussian expectations were evaluated by one-dimensional adaptive quadrature using QUADPACK [30]. For ℓ_1 regularization, the SE recursions were evaluated using the closed-form expressions involving the complementary error function.

D. Alternating Direction Method of Multipliers

We also applied ADMM [31] to log-sum-regularized reconstruction using the same adaptive-smoothing principle as in AMP. With the scaled dual variable \mathbf{u} and the ADMM penalty parameter $\rho_{\text{ADMM}} > 0$, the ADMM updates are given by

$$\tilde{\mathbf{x}}^{[t+1]} = (\mathbf{A}^\top \mathbf{A} + \rho_{\text{ADMM}} \mathbf{I})^{-1} \left(\mathbf{A}^\top \mathbf{y} + \rho_{\text{ADMM}} (\mathbf{z}^{[t]} - \mathbf{u}^{[t]}) \right), \quad (19)$$

$$\mathbf{x}^{[t+1]} = \alpha_{\text{relax}} \tilde{\mathbf{x}}^{[t+1]} + (1 - \alpha_{\text{relax}}) \mathbf{z}^{[t]}, \quad (20)$$

$$\mathbf{z}^{[t+1]} = S(\mathbf{x}^{[t+1]} + \mathbf{u}^{[t]}; (\lambda_{\text{pen}}/\rho_{\text{ADMM}}) R(\cdot)), \quad (21)$$

$$\mathbf{u}^{[t+1]} = \mathbf{u}^{[t]} + \mathbf{x}^{[t+1]} - \mathbf{z}^{[t+1]}. \quad (22)$$

Here, the relaxation step with α_{relax} was included to improve ADMM stability for the log-sum penalty. In the experiments, we set $\alpha_{\text{relax}} = 0.5$ and $\rho_{\text{ADMM}} = 1$.

It should be noted that the ADMM updates above do not necessarily reproduce the AMP dynamics. In ADMM, ε is

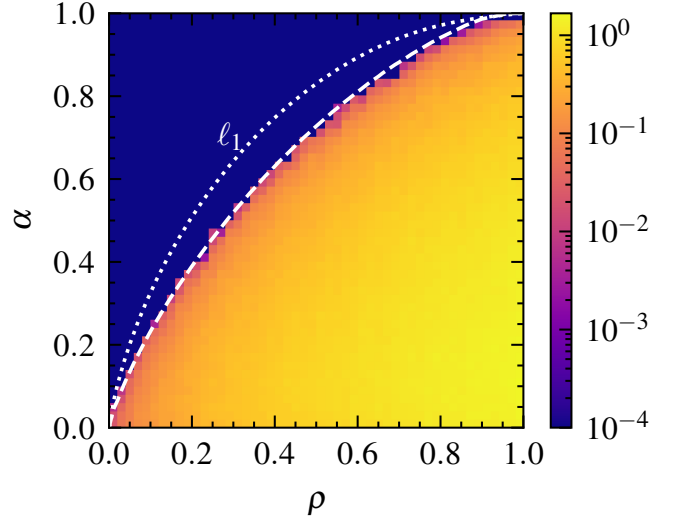


Fig. 2. MSE of ADMM reconstruction as a function of the measurement rate α and the signal density ρ in the noiseless case $\sigma^2 = 0$. The ADMM results are averaged over 5 independent trials with $N = 10^3$. The white dashed line and the white dotted line represent the predicted phase transition for the log-sum and ℓ_1 penalties, respectively.

fixed as $\varepsilon = \sqrt{\lambda_{\text{pen}}/\rho_{\text{ADMM}}}$ in the \mathbf{z} update throughout the iteration, while that for AMP changes with iteration as $\varepsilon^{[t]} = \sqrt{(\chi^{[t]} + \lambda_{\text{pen}})/\alpha}$ in the $\hat{\mathbf{x}}$ update. The ADMM experiments are therefore not intended to reproduce the AMP dynamics. Instead, they examine whether practical finite-dimensional optimization with the log-sum penalty yields reconstruction performance consistent with the SE prediction.

We also implemented ADMM for the noiseless case $\sigma^2 = 0$. In this case, we use the following algorithm corresponding to $\lambda_{\text{pen}} \rightarrow 0^+$ in (2):

$$\mathbf{x}^{[t+1]} = \mathbf{A}^\top (\mathbf{A} \mathbf{A}^\top)^{-1} \mathbf{y} + \left(\mathbf{I} - \mathbf{A}^\top (\mathbf{A} \mathbf{A}^\top)^{-1} \mathbf{A} \right) (\mathbf{z}^{[t]} - \mathbf{u}^{[t]}), \quad (23)$$

$$\mathbf{z}^{[t+1]} = S(\mathbf{x}^{[t+1]} + \mathbf{u}^{[t]}; (1/\rho_{\text{ADMM}}) R(\cdot)), \quad (24)$$

$$\mathbf{u}^{[t+1]} = \mathbf{u}^{[t]} + \mathbf{x}^{[t+1]} - \mathbf{z}^{[t+1]}. \quad (25)$$

We experimentally found that this noiseless algorithm could not be stabilized by introducing the relaxation step. Instead, we maintained stability by scheduling and adjusting the parameter ρ_{ADMM} . In the experiments, ρ_{ADMM} was initialized at 1.0 and multiplied by 1.01 at each update. In the both noisy and noiseless cases, the variables were initialized as $\mathbf{z}^{[t=0]} = \mathbf{u}^{[t=0]} = \mathbf{0}$.

III. PHASE TRANSITION IN THE NOISELESS CASE

We first analyzed the phase transition for reconstruction with log-sum regularization in the noiseless case $\sigma^2 = 0$, $\lambda_{\text{pen}} \rightarrow 0^+$. \mathbf{A} , \mathbf{x}^0 , and \mathbf{w} were generated as described in Sec. II. Reconstruction performance was evaluated by the empirical MSE

$$\text{MSE} = \frac{1}{N} \left\| \hat{\mathbf{x}} - \mathbf{x}^0 \right\|_2^2, \quad (26)$$

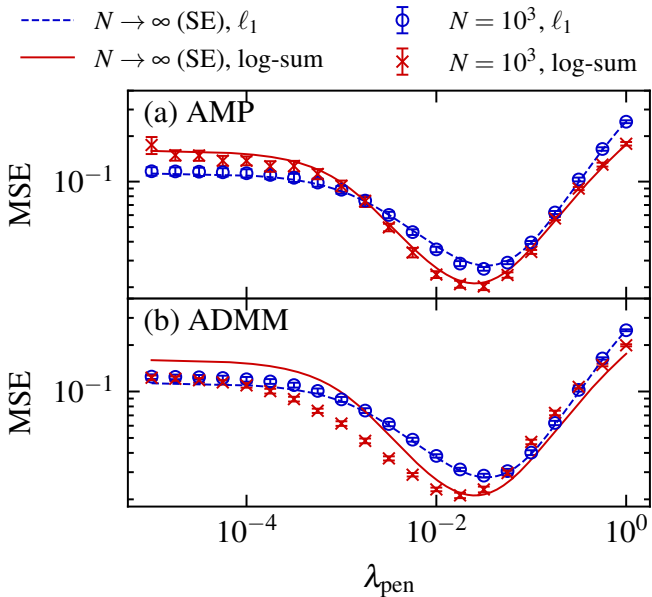


Fig. 3. Final MSE from the SE fixed-point prediction, together with (a) AMP and (b) ADMM results, as a function of λ_{pen} . The measurement rate is $\alpha = 0.9$, and the signal density is $\rho = 0.4$. The AMP and ADMM curves are averaged over 10 independent trials with $N = 10^3$.

where $\hat{\mathbf{x}}$ is the algorithmic reconstruction. In this setting, the (α, ρ) space for compressed sensing recovery in the $N \rightarrow \infty$ limit is separated by a threshold $\alpha = \alpha_c(\rho)$ into a region where the method under consideration typically achieves exact recovery, $\text{MSE} \approx 0$, and a region where it does not, $\text{MSE} > 0$.

Fig. 2 compares the ADMM experimental results with the SE prediction. ADMM experiments were run on 50×50 grids of (α, ρ) values in the ranges $\alpha \in (0, 1]$ and $\rho \in (0, 1]$. In the SE computation, for each $\rho \in (0, 1]$, the smallest α for which the MSE fell below 10^{-4} was obtained by binary search. Both ADMM and SE were run until the MSE fell below 10^{-4} or the number of iterations reached 10^3 . The typical reconstruction limit of ℓ_1 reconstruction [9] is also shown as the white dotted line for comparison. The empirically observed boundary is close to the SE prediction. In addition, the threshold $\alpha_c(\rho)$ for log-sum penalty is lower than that for ℓ_1 minimization, indicating that the log-sum version can achieve exact recovery with fewer measurements than ℓ_1 minimization.

IV. NUMERICAL EXPERIMENTS IN THE NOISY CASE

We performed experiments in the noisy case using a setting similar to the one in Sec. III, but with $\sigma^2 = 10^{-2}$ and $\lambda_{\text{pen}} > 0$. For both AMP and SE, we used damping with a damping factor of 0.2 to improve stability, and the iteration was stopped when the MSE fell below 10^{-10} or the iteration count reached 10^3 . For ADMM, the iteration was stopped when $\|z^{[t+1]} - z^{[t]}\|_2 < 10^{-10}$ and $\rho_{\text{ADMM}} \|z^{[t+1]} - z^{[t]}\|_2 < 10^{-10}$ were satisfied or the iteration count reached 10^3 .

First, we compared the SE-predicted final MSE with the algorithmic final MSEs, with particular attention to ADMM.

Unlike AMP, ADMM uses a proximal parameter $\lambda_{\text{prox}} = \lambda_{\text{pen}}/\rho_{\text{ADMM}}$ that does not change across iterations. Thus, the comparison should be interpreted as a test of whether the SE fixed point provides a useful benchmark for typical reconstruction accuracy, rather than as a trajectory-level validation of ADMM. Fig. 3 compares the final MSE as a function of the regularization coefficient λ_{pen} for the SE fixed-point prediction, AMP experiments, and ADMM experiments. For both ℓ_1 and log-sum regularization, the MSE exhibits a U-shaped dependence on the regularization parameter λ_{pen} . The AMP results agreed well with the SE prediction over a wide range of λ_{pen} . Although the ADMM results did not fully agree with the SE prediction over the entire λ_{pen} range, the ADMM minimum MSE, $(2.1 \pm 0.1) \times 10^{-2}$ where the uncertainty denotes the standard error over 10 independent trials, agreed well with the SE prediction (2.1×10^{-2}).

Next, under the same noise setting, we compared the minimum final MSEs of log-sum and ℓ_1 regularization using the SE fixed-point prediction. Fig. 4 plots the best final MSE predicted by SE in the ρ - α plane for $\alpha \in (0, 1.5]$ and $\rho \in (0, 1]$. The best final MSE was obtained by searching $\lambda_{\text{pen}} \in [10^{-4}, 10^2]$. For both penalties, the MSE decreases with increasing measurement rate α and decreasing signal density ρ . Fig. 4(c) presents the difference d in the best final MSE between the log-sum and ℓ_1 penalties on a symmetric logarithmic scale. In this plot, the region $|d| \geq 10^{-3}$ is displayed on a log scale, and the other region is shown on a linear scale. The blue region with positive values corresponds to lower MSE for the ℓ_1 penalty, and the red region with negative values corresponds to lower MSE for the log-sum penalty. This comparison shows that the relative performance of the two penalties depends on (ρ, α) . The log-sum penalty tended to yield a lower best final MSE mainly in the low- ρ or high- α region. In contrast, the ℓ_1 penalty tended to yield a lower MSE in the high- ρ and low- α region.

V. DISCUSSION AND FUTURE WORK

Our results indicate that SE predicts the noiseless phase boundary observed in the ADMM experiments and provides useful predictions for log-sum reconstruction performance. They also suggest that log-sum regularization can outperform LASSO mainly when the signal density ρ is low, or the measurement rate α is high. When ρ is high and α is low, on the other hand, LASSO can yield lower MSE. One possible explanation is that the shrinkage bias induced by ℓ_1 regularization to large components may suppress noise-induced amplitude growth, thereby unintentionally stabilizing the reconstruction.

Future work should include a more detailed analysis of the dependence on noise variance and finite-size effects. It would also be worth exploring the combination of the log-sum penalty with ℓ_2 regularization, which may provide robustness similar to that of the elastic net [32] while retaining nonconvex sparsity promotion.

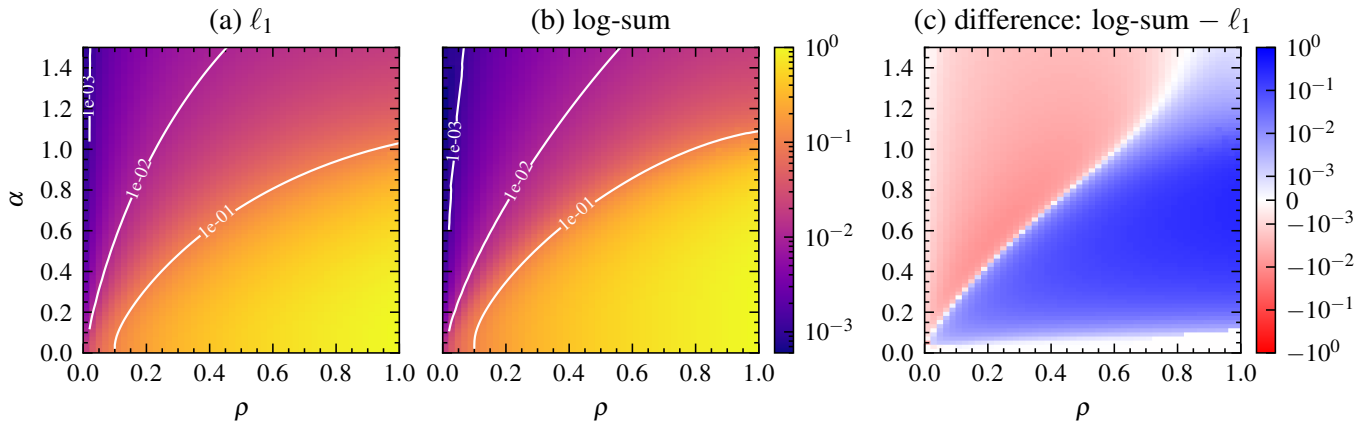


Fig. 4. Best MSE predicted by SE over $\lambda_{\text{pen}} \in [10^{-4}, 10^2]$ for (a) ℓ_1 and (b) log-sum regularization, and (c) the difference $d = \text{MSE}_{\text{logsum}} - \text{MSE}_{\ell_1}$. The noise variance is $\sigma^2 = 10^{-2}$.

VI. ACKNOWLEDGMENT

This work was supported by programs for bridging the gap between R&D and IDEal society (Society 5.0) and Generating Economic and social value (BRIDGE) and Cross-ministerial Strategic Innovation Promotion Program (SIP) from the Cabinet Office (No. 23836436).

REFERENCES

- [1] D. L. Donoho, "Compressed sensing," *IEEE Trans. Inf. Theory*, vol. 52, no. 4, pp. 1289–1306, Apr. 2006.
- [2] E. J. Candès, J. K. Romberg, and T. Tao, "Stable signal recovery from incomplete and inaccurate measurements," *Commun. Pure Appl. Math.*, vol. 59, no. 8, pp. 1207–1223, Aug. 2006.
- [3] Y. Wiaux, L. Jacques, G. Puy, A. M. M. Scaife, and P. Vanderghyest, "Compressed sensing imaging techniques for radio interferometry," *Mon. Not. R. Astron. Soc.*, vol. 395, no. 3, pp. 1733–1742, 21 May 2009.
- [4] F. J. Herrmann and G. Hennenfent, "Non-parametric seismic data recovery with curvelet frames," *Geophys. J. Int.*, vol. 173, no. 1, pp. 233–248, 1 Apr. 2008.
- [5] Z. Qin, J. Fan, Y. Liu, Y. Gao, and G. Y. Li, "Sparse representation for wireless communications: A compressive sensing approach," *IEEE Signal Processing Magazine*, vol. 35, no. 3, pp. 40–58, 2018.
- [6] M. Lustig, D. Donoho, and J. M. Pauly, "Sparse MRI: The application of compressed sensing for rapid MR imaging," *Magn. Reson. Med.*, vol. 58, no. 6, pp. 1182–1195, Dec. 2007.
- [7] R. Tibshirani, "Regression shrinkage and selection via the lasso," *J. R. Stat. Soc. Series B Stat. Methodol.*, vol. 58, no. 1, pp. 267–288, 1 Jan. 1996.
- [8] S. Rangan, V. Goyal, and A. K. Fletcher, "Asymptotic analysis of MAP estimation via the replica method and compressed sensing," in *Advances in Neural Information Processing Systems*, Y. Bengio, D. Schuurmans, J. Lafferty, C. Williams, and A. Culotta, Eds., vol. 22. Curran Associates, Inc., 2009.
- [9] Y. Kabashima, T. Wadayama, and T. Tanaka, "A typical reconstruction limit for compressed sensing based on L_p -norm minimization," *J. Stat. Mech.*, vol. 2009, no. 09, p. L09003, 21 Sep. 2009.
- [10] S. Ganguli and H. Sompolinsky, "Statistical mechanics of compressed sensing," *Phys. Rev. Lett.*, vol. 104, no. 18, p. 188701, 7 May 2010.
- [11] F. Krzakala, M. Mézard, F. Sausset, Y. F. Sun, and L. Zdeborová, "Statistical-physics-based reconstruction in compressed sensing," *Phys. Rev. X.*, vol. 2, no. 2, p. 021005, 11 May 2012.
- [12] J. Fan and R. Li, "Variable selection via nonconcave penalized likelihood and its oracle properties," *J. Am. Stat. Assoc.*, vol. 96, no. 456, pp. 1348–1360, Dec. 2001.
- [13] H. Zou, "The adaptive lasso and its oracle properties," *J. Am. Stat. Assoc.*, vol. 101, no. 476, pp. 1418–1429, 1 Dec. 2006.
- [14] R. Chartrand, "Exact reconstruction of sparse signals via nonconvex minimization," *IEEE Signal Processing Letters*, vol. 14, no. 10, pp. 707–710, Oct. 2007.
- [15] R. Chartrand and W. Yin, "Iteratively reweighted algorithms for compressive sensing," in *2008 IEEE International Conference on Acoustics, Speech and Signal Processing*. IEEE, 4 Mar. 2008, pp. 3869–3872.
- [16] E. J. Candès, M. B. Wakin, and S. P. Boyd, "Enhancing sparsity by reweighted ℓ_1 minimization," *J. Fourier Anal. Appl.*, vol. 14, no. 5-6, pp. 877–905, 15 Dec. 2008.
- [17] Y. Shen, J. Fang, and H. Li, "Exact reconstruction analysis of log-sum minimization for compressed sensing," *IEEE Signal Process. Lett.*, vol. 20, no. 12, pp. 1223–1226, Dec. 2013.
- [18] A. Prater-Bennette, L. Shen, and E. E. Tripp, "The proximity operator of the log-sum penalty," *J. Sci. Comput.*, vol. 93, no. 3, p. 67, 25 Dec. 2022.
- [19] C.-H. Zhang, "Nearly unbiased variable selection under minimax concave penalty," *Ann. Stat.*, vol. 38, no. 2, pp. 894–942, 1 Apr. 2010.
- [20] T. Furuhashi, H. Hontani, Q. Zhao, and T. Yokota, "WEPP: A differentiable nonconvex sparse regularizer via weakly-convex envelope," *arXiv [cs.LG]*, 19 Jan. 2026.
- [21] R. Chartrand and V. Staneva, "Restricted isometry properties and non-convex compressive sensing," *Inverse Probl.*, vol. 24, no. 3, p. 035020, 1 Jun. 2008.
- [22] S. Foucart and M.-J. Lai, "Sparsest solutions of underdetermined linear systems via ℓ_q -minimization for $0 < q \leq 1$," *Appl. Comput. Harmon. Anal.*, vol. 26, no. 3, pp. 395–407, May 2009.
- [23] A. Sakata and Y. Xu, "Approximate message passing for nonconvex sparse regularization with stability and asymptotic analysis," *J. Stat. Mech.*, vol. 2018, no. 3, p. 033404, 13 Mar. 2018.
- [24] A. Sakata and T. Obuchi, "Perfect reconstruction of sparse signals with piecewise continuous nonconvex penalties and nonconvexity control," *J. Stat. Mech.*, vol. 2021, no. 9, p. 093401, 1 Sep. 2021.
- [25] X. Gu, A. Sakata, and T. Obuchi, "Perfect reconstruction of sparse signals using nonconvexity control and one-step RSB message passing," *arXiv [stat.ML]*, 19 Dec. 2025.
- [26] K. Morita, F. Ricci-Tersenghi, and M. Ohzeki, "Phase transition in compressed sensing using log-sum penalty and adaptive smoothing," *arXiv [cs.IT]*, 15 Apr. 2026.
- [27] M. Mezard, G. Parisi, and M. A. Virasoro, *Spin glass theory and beyond: An introduction to the replica method and its applications: An introduction to the replica method and its applications*, ser. World Scientific Lecture Notes In Physics. Singapore, Singapore: World Scientific Publishing, 11 Jan. 1987.
- [28] D. L. Donoho, A. Maleki, and A. Montanari, "Message-passing algorithms for compressed sensing," *Proc. Natl. Acad. Sci. U. S. A.*, vol. 106, no. 45, pp. 18 914–18 919, 10 Nov. 2009.
- [29] M. Bayati and A. Montanari, "The dynamics of message passing on dense graphs, with applications to compressed sensing," *IEEE Trans. Inf. Theory*, vol. 57, no. 2, pp. 764–785, Feb. 2011.

- [30] R. Piessens, E. D. Doncker-Kapenga, C. Uberhuber, and D. K. Kahaner, *Quadpack: A subroutine package for automatic integration*, ser. Springer Series in Computational Mathematics. Berlin, Germany: Springer, 1 Jul. 1983.
- [31] S. Boyd, "Distributed optimization and statistical learning via the alternating direction method of multipliers," *Found. Trends® Mach. Learn.*, vol. 3, no. 1, pp. 1–122, 2010.
- [32] H. Zou and T. Hastie, "Regularization and variable selection via the elastic net," *J. R. Stat. Soc. Series B Stat. Methodol.*, vol. 67, no. 2, pp. 301–320, 1 Apr. 2005.